Journal of the Physical Society of Japan
Vol. 53, No. 5, May, 1984, pp. 1746–1752

Antenna Loading and Electron Heating Experiments of ICRF Wave in TNT-A Tokamak

Shunjiro SHINOHARA, Nobuyuki ASAKURA,
Masahiro NAITO and Kenro MIYAMOTO

Department of Physics, Faculty of Science,
University of Tokyo, Bunkyo-ku, Tokyo 113

(Received September 22, 1983)

Antenna loading resistance and electron heating effects of ICRF wave were investigated in TNT-A tokamak. Lodaing resistance increased with the mean plasma density and decreased with the input power. The effect of the distance between the plasma and antenna surface on loading resistance was studied and had good agreements with the calculated results. The increase in the soft Xray emissivity was larger in the presence of ion-ion hybrid and/or ion cyclotron resonance layer in the plasma than that in the absence of them. With the absorbed power up to two times of the ohmic power, the central electron temperature increased by 20%, the soft Xray emissivity increased by 80% and the mean plasma density decreased by 10%, while the total radiation loss increased slightly (by 15%).

§1. Introduction

It is acknowledged that RF heating in the ion cyclotron range of frequency (ICRF)[1] is a promising heating method in tokamaks.[2] Steady progress has been made as to the high efficiency of ion heating rate with the high RF power.[3-6]

Physics of the wave excitation, propagation and absorption is being actively studied. It is also important to study antenna-plasma coupling relating the efficiency of energy transfer from the exciting system, and heating effects for various antenna configurations and plasma parameters. Experimental results on the dependence of loading resistance indicating antenna-plasma coupling are not sufficient.[7-9] Roles of resonance layers on the plasma heating must be also investigated in detail.

Here, loading resistance and electron heating effects in TNT-A[10,11] are reported. In §2 the antenna structure is described. Parameter dependence of loading resistance (plasma density, mode excitation and distance between plasma and antenna surface) is presented in §3. Heating effects from the view point of the electron heating under the various conditions are studied in §4, and conclusions are presented in §5.

§2. Antenna Structure

In TNT-A, the vacuum chamber made of stainless steel has a rectangular cross section, 60 cm high and 24 cm wide, and nine flux loops and many magnetic probes are located

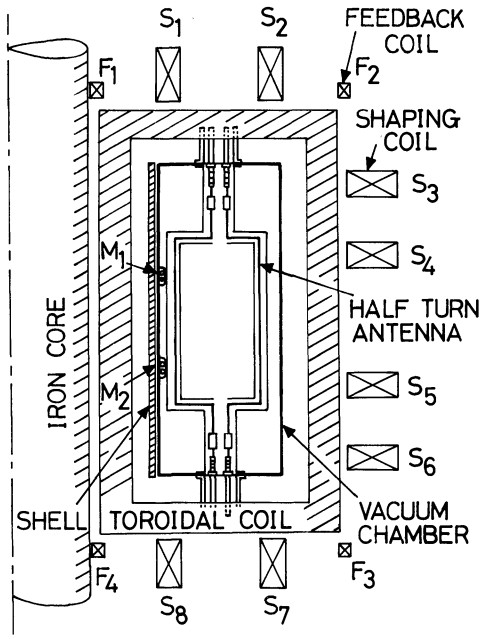

Fig. 1. Cross-sectional view of TNT-A. Two half-turn antennas are located on the high and low field sides inside the vacuum chamber.

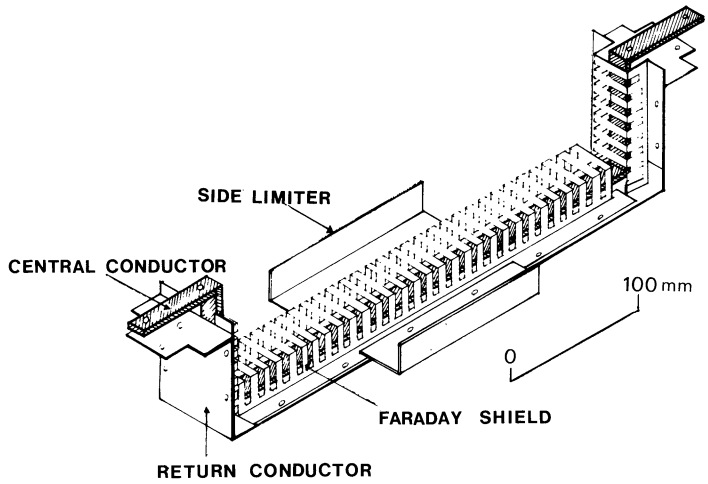

Fig. 2. Schematic view of half-turn antenna. The central conductor of copper has a rectangular cross section, 0.3 cm thick and 1.2 cm wide, and other parts are made of stainless steel with 0.1 cm thickness. Faraday shield was used to reduce the toroidal electric field. Each strip is 0.6 cm wide and each gap has 0.4 cm width in one screen. Side limiters protect the antenna from the damage by the plasma.

inside the chamber. Two half-turn antennas, which form the rectangular cross section, are located on the high and low field sides inside the chamber, as shown in Fig. 1. By changing the connection of the feedthrough of the antenna, four ways of the excitation are possible; high field side only, low field side only, $m=\pm 1$ mode (parallel connection of the antennas) and $m=0$ mode (series connection of the antennas) excitation (m is the poloidal mode number).

Figure 2 shows the schematic view of the half-turn antenna. The central conductor of copper has a rectangular cross section, 0.3 cm thick and 1.2 cm wide, and other parts are made of stainless steel with 0.1 cm thickness. Faraday shield was used to reduce the excited toroidal electric field. Each strip of Faraday shield is 0.6 cm wide and each gap has 0.4 cm width. Generally two screens of Faraday shield are provided, but in these experiments only one screen was used in most cases. The height of side limiters which protect the antennas from the damage by the plasma was the same with that of the screen surface. Both ends of return conductor are connected to the vacuum chamber.

The frequencies of the generator were 4.5 and 5.6 MHz, the pulse width was up to 10 ms and the maximum power of the generator was 200 kW.

§3. Loading Resistance

Typical plasma parameters in these experiments were as follows; major radius $R_0=40$ cm, minor radius $a=7.5$ cm, elongation ratio $\kappa=1.2$, toroidal field $B_t=4$ kG, plasma current $I_p=5$ kA, loop voltage $V_l=5$ V, mean plasma density $\bar{n}_e=10^{13}$ cm^{-3} and central electron temperature $T_e(0)=70$ eV.

Loading resistance R was defined as $R=P_{inp}/I^2$, where P_{inp} is the input power from the generator and I is the antenna current. When two antennas were used ($m=0$ or $m=\pm 1$ mode excitation), we added two values of loading resistance of each antenna for the comparison with the calculated results.

Firstly, the dependence of loading resistance on the input power was studied, as shown in Fig. 3, in the case of low field side excitation. Here, R_c is vacuum loading resistance and P_{net} is the net power absorbed by the plasma defined as $P_{net}=P_{inp}\times(R-R_c)/R=P_{inp}\times R_p/R$ (R: total loading resistance in the presence of the plasma $=R_c+R_p$, R_p: plasma loading resistance). Figure 3 shows that loading resistance R decreased with the increase in the input power P_{inp}, and R/R_c became $\simeq 2$ with $P_{inp}\simeq 60$ kW. The net power P_{net} was up to 30 kW.

The cause of the decrease in loading resistance with the input power was not clear,

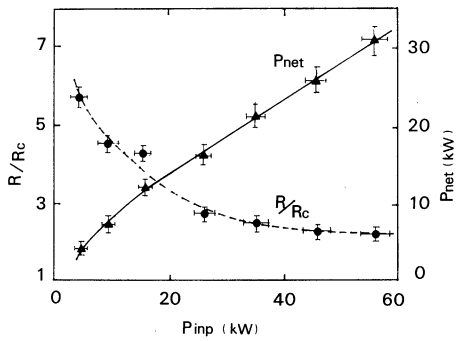

Fig. 3. Dependence of normalized loading resistance R/R_c and net power P_{net} on input power P_{inp} in the case of low field side excitation (R: total loading resistance $=R_c+R_p$, R_c: vacuum loading resistance, R_p: plasma loading resistance).

but the plasma parameters near the antenna seemed to play an important role. With the increase in the input power, the increase in the electron temperature and the decrease in the plasma density near the antenna were observed by the Langmuir probe's measurements.

Figure 4 shows the relation between loading resistance and the mean plasma density in the case of $m=0$ mode excitation. With the increase in the mean plasma density $\bar{n}_e$, loading resistance increased as expected.[12,13] (These codes with a slab model from refs. 12 and 13 well explain plasma loading experimentally obtained in many machines.) Below $\bar{n}_e \simeq 2\times 10^{12}$ cm^{-3}, loading resistance was almost the same with vacuum loading resistance. From Fig. 4, high density operation is favourable, because P_{net}/P_{inp} is larger (efficiency of power absorption by the plasma is higher) and the voltage at the feedthrough becomes lower (at the given voltage determined by the breakdown, the maximum input power becomes higher).

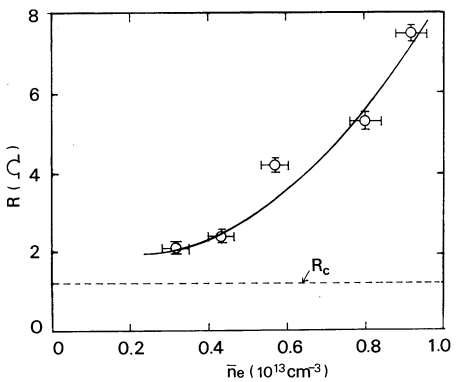

Fig. 4. Dependence of loading resistance R on the mean plasma density $\bar{n}_e$ in the case of $m=0$ mode excitation and $P_{inp}\simeq 40$ kW.

The distance between the plasma and antenna surface is an important parameter of RF loading resistance for the design of the antenna in future tokamaks. The dependence of plasma loading resistance on this distance was studied, as shown in Fig. 5. In the case of low field side excitation, we changed the distance by inserting the movable limiter, made of stainless steel (6 cm high and 0.3 cm thick), which was 90° toroidally away from the antenna. The change of plasma loading resistance R_p with the distance Δx between the surfaces of the antenna and the movable limiter was not large, and the small dip at $\Delta x \simeq -1$ cm indicated the cavity mode of this wave. The calculated results of loading resistance using the hot slab model including the collision from ref. 13 well described the experimental results.

The increase in loading resistance with the plasma current was found, and loading resistance with two screens of Faraday shield was less than that with one screen.

These features are considered to be due to the change of the plasma density near the

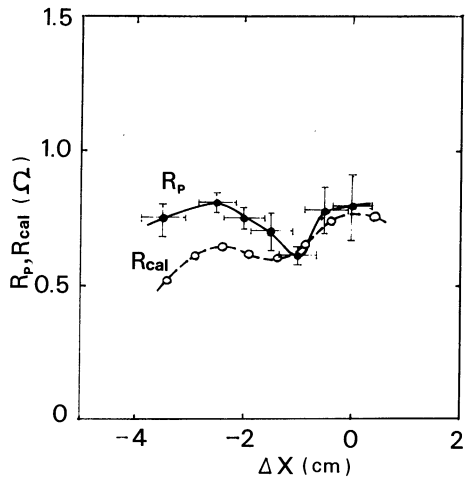

Fig. 5. Dependence of experimental (R_p) and calculated (R_{cal}) plasma loading resistance on the distance Δx between the surfaces of the plasma and movable limiter with $\bar{n}_e \simeq 10^{13}$ cm^{-3} and $P_{inp}\simeq$ 40 kW. The positive value of Δx means that the movable limiter is outside the antenna surface in the major radius.

antenna surface. (In general, loading resistance decreases with the decrease in the plasma density near the antenna.)

Loading resistance changed a little by varying the toroidal field B_t and the ratio of hydrogen to deuterium density n_H/n_D. This indicated that the collision in TNT-A plasma could not be neglected.

The values of plasma loading resistance R_p were $\sim 0.6\,\Omega$, $\sim 0.8\,\Omega$, $\sim 5\,\Omega$ and $\sim 4\,\Omega$ in the case of high field, low field, $m=\pm 1$ and $m=0$ mode excitation, respectively, with $P_{inp}=30-40$ kW, $\bar{n}_e \simeq 8\times 10^{12}$ cm^{-3}, $I_p=4-5$ kA and frequency $f=5.6$ MHz.

Plasma loading resistance in the case of $m=\pm 1$ mode excitation was larger than the sum of that in the case of high and low field side excitation with the same input power. This was partly because the input power per each antenna in the case of $m=\pm 1$ mode excitation was nearly as half as that in the case of high or low field side excitation only.

Plasma loading resistance in the case of $m=0$ mode excitation was larger than the calculated value, using the code from ref. 13. The discrepancy between the experimental and calculated value was not clear, but the calculated results show that the electric field parallel to the current at one antenna surface (this field is proportional to loading resistance) is lowered by the other antenna because of the strong interference between two antennas in the case of $m=0$ mode excitation.

To sum up, experimental plasma loading resistance for various excitations did not change appreciably with the same input power in each antenna. This was thought to be due to the relatively low density plasma of $\sim 10^{13}$ cm^{-3} and the weak toroidal field of ~ 4 kG (i.e., excited wavelength > machine size), and the collisional damping.

§4. Electron Heating Effects

In the ion-ion hybrid resonance regime, the fast wave[14] is converted into an ion Bernstein wave near the hybrid resonance layer and the wave energy is transferred to the three kinds of particles;[15,16] protons (cyclotron damping), deuterons (harmonic cyclotron damping) and electrons (Landau damping). The coupling to an ion Bernstein wave occurs also near the second harmonic resonance layer.[17] (The condition of Landau damping (electron thermal velocity of $\sim 3\times 10^6$ m/s equals phase velocity along the magnetic field) was satisfied in TNT-A.) The collisional damping between

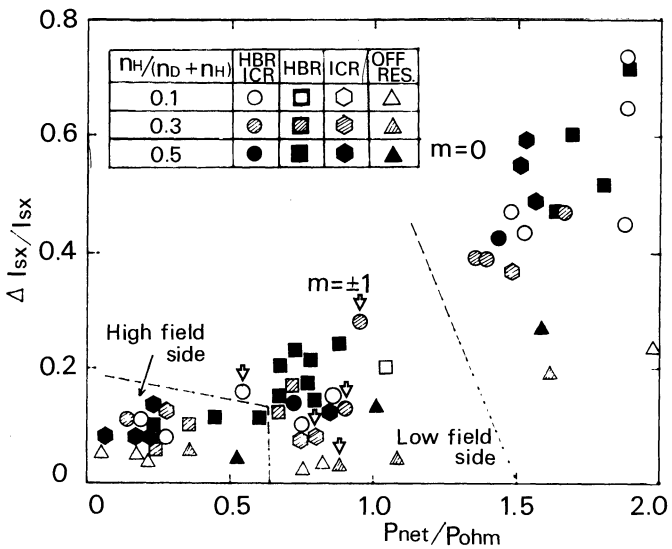

Fig. 6. Relative change of soft X-ray emissivity $\Delta I_{sx}/I_{sx}$ from the plasma core vs net power P_{net} normalized by ohmic power P_{ohm} under the various conditions. Here, n_H and n_D are hydrogen and deuterium density, respectively. When ion-ion hybrid and ion cyclotron resonance layers (fundamental for protons and second harmonic for deuterons) are present in the plasma, we denote HBR and ICR, respectively.

charged particles and neutrals cannot be neglected in this machine.

The electron heating by ICRF wave was studied by varying the ratio of hydrogen to deuterium density, toroidal field and excitation modes. It is important to examine the conditions of the electron heating, especially in the case of non-circular plasma as the power deposition profile affects elongation ratio through the current density profile.[11] (There was no diagnostics to measure the ion temperature.)

In order to investigate the electron heating effects, we used the silicon surface barrier diode to observe the soft X ray emissivity. By the use of the polypropylene, 1 μm thick, as a filter, the energy above 150 eV could be detected.

Figure 6 shows the dependence of the relative change of the soft X ray intensity on the net power P_{net} normalized by the ohmic power P_{ohm} under the various conditions. The appreciable difference in this dependence was not found by changing the ratio of hydrogen to deuterium density. However, the increase in the soft X ray emissivity was larger in the presence of ion-ion hybrid and/or ion cyclotron resonance layer in the plasma than that in the absence of them. (The collisional electron heating (off resonance heating) is about one third of the total electron heating in the presence of the resonance layer.) The soft

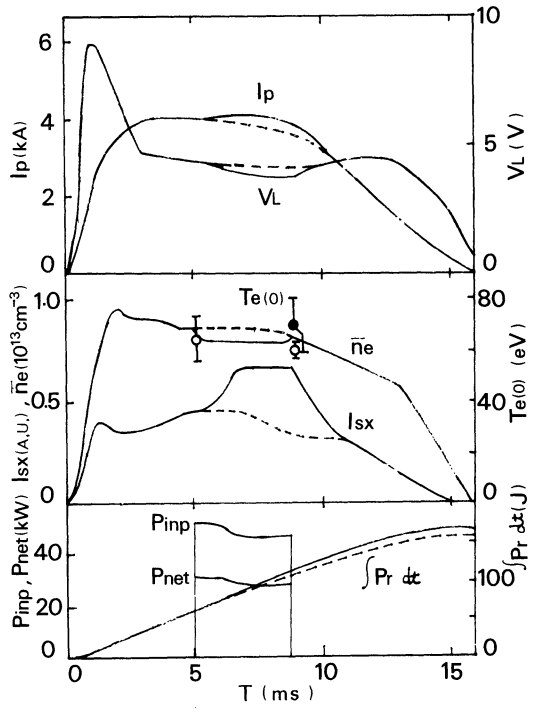

Fig. 7. Time evoltuion of plasma current I_p, loop voltage V_l, soft Xray emissivity I_{sx}, mean plasma density $\bar{n}_e$, central electron temperature $T_e(0)$ by the Thomson scattering, input power P_{inp}, net power P_{net} and time integrated total radiation loss $\int P_r dt$ by the bolometer. Solid lines and closed circles, broken lines and open circles show the cases with and without the RF power, respectively. In this discharge, $m=0$ mode excitation was tried in the presence of only ion-ion hybrid resonance layer in the plasma.

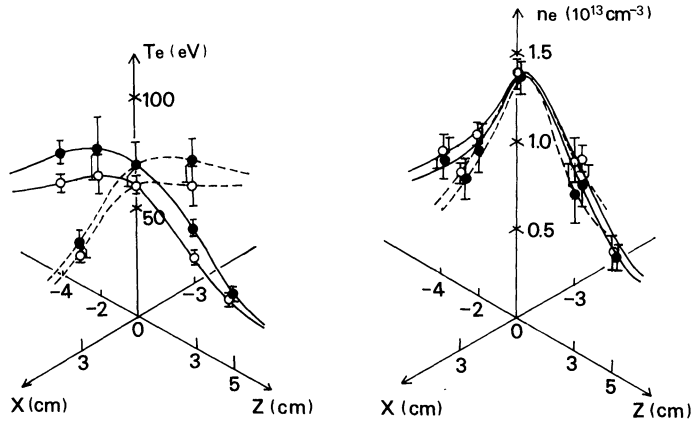

Fig. 8. Two-dimensional distribution of electron temperature T_e and density n_e by the Thomson scattering with (closed circles) and without (open circles) the RF power at $t=8.9$ ms, with same parameters in Fig. 7. Absolute values of electron density were derived by the use of 4 mm microwave interferometer. Here, x and z are taken along the radial and vertical directions, respectively.

X-ray intensity in the presence of resonance layer increased with the increase in P_{net}/P_{ohm}.

Figure 7 shows the typical example of time evolution of plasma parameters with and without the RF power in the presence of ion-ion hybrid resonance layer only ($m=0$ mode excitation). With the net power P_{net} of 1.7 times as large as the ohmic power P_{ohm}, the conductivity, central electron temperature and soft X ray emissivity increased by 15%, 15% and 80%, respectively. The mean plasma density decreased by 10% and the appreciable enhancement of impurity radiation was not found (total radiation loss increased only by 15%).

In the presence of ion-ion hybrid and ion cyclotron resonance layer in the plasma, the same effects were found. With $P_{net}/P_{ohm}\simeq 2$ in the case of $m=0$ mode excitation, the conductivity, central electron temperature and soft X ray emissivity increased by 10%, 25% and 75%, respectively, while the mean plasma density decreased by 5%.

Two-dimensional distribution of the electron temperature and density was measured by the Thomson scattering, as shown in Fig. 8, with the same parameters as in Fig. 7. The increase in the electron temperature was observed over the plasma cross section, especially the increase near the plasma center was larger, while the electron density decreased a little.

From these measurements, the electron heating was effective in the presence of ion-ion hybrid and/or ion cyclotron resonance layer in the plasma, which was considered to be due to the electron Landau damping and energy transfer from ions, while the role of the collisional (off resonance) heating was small.

§5. Conclusions

Antenna loading resistance and heating effects were measured under the various conditions in TNT-A tokamak. Loading resistance increased with the mean plasma density ($<1.3\times10^{13}$ cm^{-3}), but decreased with the input power (<80 kW). The values of plasma loading resistance were $\sim0.6\,\Omega$, $\sim0.8\,\Omega$, $\sim5\,\Omega$ and $\sim4\,\Omega$ in the case of high field, low field, $m=\pm1$ and $m=0$ mode excitation, respectively, under the same conditions of $P_{inp}=30-40$ kW, $\bar{n}_e\simeq8\times10^{12}$ cm^{-3}, $I_p=4-5$ kA and $f=5.6$ MHz. With the same input power in each antenna, plasma loading resistance did not change appreciably for various excitations.

The effect of the distance between the plasma and antenna surface on loading resistance was investigated and had good agreements with the calculated results using the hot slab model including the collision.

The importance of resonance layers on the electron heating was confirmed and the role of the collisional damping was small. The intensity of the soft X ray emissivity by the silicon surface barrier diode was stronger in the presence of ion-ion hybrid and/or ion cyclotron resonance layer in the plasma than that in the absence of them. In the presence of the resonance layer, the soft X ray intensity increased with the increase in P_{net}/P_{ohm}.

The electron heating was also observed from the two-dimensional measurements of the electron temperature and density by the Thomson scattering in the presence of ion-ion hybrid resonance layer only, and ion-ion hybrid and ion-cyclotron resonance layer. With the net power up to two times of the ohmic power, the conductivity, central electron temperature and soft X ray emissivity increased by 15%, 20% and 80%, respectively. The mean plasma density decreased by 10%, while the radiation loss increased slightly (by 15%).

Acknowledgements

We would like to thank Mr. K. Ida for his helpful discussion and thank Mr. I. Ochiai and Dr. Y. Nagayama for their help in the Thomson scattering system.

References

1) T. H. Stix: Nucl. Fusion **15** (1975) 737.
2) INTOR Group: Nucl. Fusion **20** (1980) 349.
3) D. Hwang *et al.*: in *Plasma Physics and Controlled Nuclear Fusion Reseacrh* (Proc. 9th Int. Conf., Baltimore, 1982) **2** (1983) 3.
4) TFR Group, A. Trunc and D. Gresillon: in *Plasma Physics and Controlled Nuclear Fusion Research* (Proc. 9th Int. Conf., Baltimore, 1982) **2** (1983) 17.
5) H. Kimura *et al.*: in *Plasma Physics and Controlled Nuclear Fusion Research* (Proc. 9th Int. Conf., Baltimore, 1982) **2** (1983) 113.

6) T. Amano *et al.*: in *Plasma Physics and Controlled Nuclear Fusion Research* (Proc. 9th Int. Conf., Baltimore) **1** (1983) 219.
7) EQUIPE TFR: CEA-Euratom Report, EUR-CEA-FC-1115 (1981).
8) H. Kimura *et al.*: JAERI-M 82-046 (1982).
9) M. Ichimura *et al.*: Proc. Int. Conf. on Plasma Physics **1** (1982) 125.
10) S. Shinohara, K. Sakuma, Y. Nagayama and H. Toyama: J. Phys. Soc. Jpn. **52** (1983) 94.
11) S. Shinohara, I. Ochiai, S. Tsuji, H. Toyama and K. Miyamoto: J. Phys. Soc. Jpn. **52** (1983) 364.
12) S. Shinohara, M. Naito and K. Miyamoto: J. Phys. Soc. Jpn. **52** (1983) 2622.
13) A. Fukuyama, S. Nishiyama, K. Itoh and S. I. Itoh: Nucl. Fusion **23** (1983) 1005.
14) K. Ida, O. Naito, S. Shinohara and K. Miyamoto: Nucl. Fusion **23** (1983) 1259.
15) D. G. Swanson: Phys. Rev. Lett. **36** (1976) 316.
16) F. W. Perkins: Nucl. Fusion **19** (1979) 461.
17) R. R. Wehnants: Phys. Rev. Lett. **33** (1974) 78.